Analysis and Operation of Modular Multilevel Converters With Phase-Shifted Carrier PWM

Kalle Ilves, *Student Member, IEEE*, Lennart Harnefors, *Senior Member, IEEE*, Staffan Norrga, *Member, IEEE*, and Hans-Peter Nee, *Senior Member, IEEE*

***Abstract*—Many publications have been presented on the modulation and control of the modular multilevel converter, some of which are based on phase-shifted carrier modulation. This paper presents an analysis of how the switching frequency affects the capacitor voltages, circulating currents, and alternating voltages using phase-shifted carrier modulation. It is found that switching frequencies that are integer multiples of the fundamental frequency should be avoided as they can cause the capacitor voltages to diverge. Suitable switching frequencies are derived for which the arm and line quantities will be periodic with symmetric operating conditions in the upper and lower arms. Thus, the practical outcome of this paper is a detailed description of how the switching frequency should be chosen in order to achieve advantageous operating conditions. The theoretical results from the analysis are validated by both simulations and experimental results.**

***Index Terms*—Capacitor voltages, circulating current, modular multilevel converter (M2C), phase-shifted PWM, switching harmonics.**

NOMENCLATURE

β	Angular displacement of the upper arm carrier waveforms with respect to the lower arm.
$\hat{i}_{hl,u}$	Amplitude of the harmonic component with the frequency ω_h.
ω_1	Fundamental frequency.
ω_c	Carrier frequency.
ω_h	Angular frequency of the harmonic components which appear in the arm currents.
$\theta_{kl,u}$	Angular displacement of the carrier waveform in submodule k.
$\varphi_{hl,u}$	Phase angle of the harmonic component with the angular frequency ω_h.
$A_{abkl,u}$	Switching harmonic of submodule k.
C	Submodule capacitance.
i_c	Instantaneous value of the circulating current.
i_d	Time-average of the circulating current.
$i_{l,u}$	Instantanous value of the arm current.
i_{ce}	Even-order harmonic components in the circulating current.
i_{cso}	Subharmonics and odd-order harmonic components in the circulating current.
i_s	Instantaneous value of ac-side current.
$i_{\mathrm{cap},kl,u}$	Capacitor current in submodule k.
J_b	Bessel function of the first kind.
L	Arm inductance.
m	Modulation index.
N	Number of submodules per arm.
$n_{l,u}$	Insertion index.
R	Arm resistance.
$s_{hl,u}$	Switching harmonics which are not canceled out in the ideal multilevel waveform.
$s_{kl,u}$	Switching function of submodule k.
$s_{l,u}^{\Sigma}$	Sum of all switching functions in one arm.
t	Time.
v_d	Dc-link voltage.
v_s	Voltage at ac terminal.
$v_{cal,u}$	Average capacitor voltage variation in one arm.
$v_{cl,u}^{\Sigma}$	Sum of all capacitor voltages in one arm.
$v_{cskl,u}$	Individual capacitor voltage variation in submodule k.
$V_{kl,u}$	Initial value of the capacitor voltage in submodule k.
$v_{l,u}$	Inserted arm voltage.
$v_{\mathrm{cap},kl,u}$	Capacitor voltage in submodule k.

The indices l and u indicate lower and upper arm quantities, respectively.

Manuscript received September 29, 2013; revised April 20, 2014; accepted April 28, 2014. Date of publication April 29, 2014; date of current version August 26, 2014. This paper was presented at the IEEE Energy Conversion Congress and Exposition Sep. 15–19, 2013, Denver, CO, USA. Recommended for publication by Associate Editor J. Mahseredjian.

K. Ilves, S. Norrga, and H.-P. Nee are with the Electrical Energy Conversion Laboratory, Royal Institute of Technology (KTH) SE-10044 Stockholm, Sweden (e-mail: ilves@kth.se; norrga@kth.se; hansi@kth.se).

L. Harnefors is with the ABB Corporate Research Center, SE-72178 Vasteras, Sweden (e-mail: lennart.harnefors@se.abb.com).

Color versions of one or more of the figures in this paper are available online at http://ieeexplore.ieee.org.

Digital Object Identifier 10.1109/TPEL.2014.2321049

I. INTRODUCTION

THE modular multilevel converter (M2C), presented in [1], is a cascaded converter topology suitable for high-voltage high-power applications such as high-voltage dc transmission [2], [3], high-power motor drives [4]–[7], and electric railway supplies [8], [9]. A multitude of dynamic models of the M2C [10]–[13] have been proposed since it was first introduced in [1]. The dynamics of the M2C are, however, time variant [13], and explicit solutions may not always be possible to find. In [14], the circulating current at direct modulation was derived analytically and resonant frequencies could be identified. The analysis in [14] did, however, not include the effect of switching harmonics. Since the M2C can operate at very low switching frequencies, even at the fundamental frequency [15], the impact of switching harmonics must be considered in order to fully understand the interaction of the main-circuit design and the control system. There are, however, numerous modulation methods that have been considered in the literature. These modulation methods may include different types of multilevel pulse

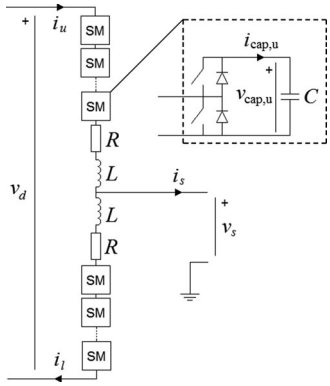

Fig. 1. Schematic diagram of one phase leg of the M2C and the circuit diagram of one submodule.

width modulation [16], nearest-level modulation [17], [18], predictive control [19], and tolerance band-based methods [20]. In many cases, there is a feed-back type control of the capacitor voltages that involves some kind of sorting such as the sorting algorithm presented in [1]. In these cases, the submodule that is inserted is determined in a stochastic manner and the system becomes difficult to analyze with analytical methods. However, if phase-shifted carrier modulation [21] is used, the system becomes deterministic and its characteristics and potential problems are more easily analyzed. The switching harmonics that appear on the dc link if the upper and lower arm submodules are not switched in a complementary manner were considered in [22] and [23]. A detailed analysis that investigates the interaction between the switching harmonics, capacitor voltages, and arm and line quantities have, however, not yet been presented. This paper provides an analytical analysis of how the switching harmonics influence the individual capacitor voltages and identifies potential problems at certain switching frequencies. The analysis also investigates how the capacitor voltage variations and switching harmonics affects the circulating currents and alternating voltages. Based on the findings, suitable switching frequencies can be identified for which the arm and line quantities will be periodic and the capacitor voltages can be kept balanced with symmetric operating conditions in the upper and lower arms.

The outline of this paper is as follows. Section II gives a short introduction to the topology and its operating principles. Phase-shifted carrier modulation is then described in more detail in Section III. Section IV provides an investigation of how the voltages and currents are affected by the carrier frequency. The theoretical findings are then validated by simulations and experiments in Section V. Finally, conclusions are presented in Section VI.

II. Operating Principles and Terminology

A schematic diagram of one phase leg of the M2C is shown in Fig. 1. Each phase leg consists of two arms connected in series between the dc terminals. Each arm consists of N series-connected half-bridges, termed submodules. As shown in Fig. 1, the submodules are equipped with dc capacitors. Each arm also has one arm inductor with the inductance L connected in series with the submodules. The purpose of the arm inductors is to limit parasitic currents and fault currents [24], [25]. The losses in the converter are modeled by the resistance R in each arm.

The converter is controlled in such way that the voltages across the submodule capacitors remain close to their nominal values. In this way, the capacitors act as voltage sources that can be inserted and bypassed in the chain of series-connected submodules. This means that an alternating voltage can be obtained by varying the number of inserted submodules in each arm, and thus, an alternating voltage with an offset is generated. If the alternating voltage is in antiphase in the upper and lower arms, a direct voltage is imposed between the dc terminals and an alternating voltage is generated at the ac terminal.

The insertion indices indicating the relative number of submodules that should be inserted in the each arm are denoted n_l for the lower arm and n_u for the upper arm. Typically, n_l and n_u are varying sinusoidally, but in many practical applications, they may also contain additional harmonic components such as a third-order harmonic in order to increase the maximum possible modulation index. The insertion indices can also be adjusted in order to compensate for the capacitor voltage ripple or inject harmonic components in the circulating current. However, in order to simplify the analysis, it is assumed that the insertion indices are sinusoidal waveforms with dc-offsets. Accordingly

$$n_l = \frac{1}{2}[1 + m\cos(\omega_1 t)] \tag{1a}$$

$$n_u = \frac{1}{2}[1 - m\cos(\omega_1 t)] \tag{1b}$$

where ω_1 is the angular fundamental frequency, m is the modulation index, defined as the peak-to-peak value of the alternating voltage divided by the pole-to-pole voltage of the dc link.

The current flowing in each arm is denoted as i_l for the lower arm and i_u for the upper arm. The arm currents are defined such that a positive arm current is charging the capacitors. Consequently, the currents i_l and i_u in Fig. 1 are given by

$$i_l = i_c - \frac{1}{2}i_s \tag{2a}$$

$$i_u = i_c + \frac{1}{2}i_s \tag{2b}$$

where i_c is the circulating current flowing between the dc terminals and i_s is the output current flowing through the ac terminal. The direct component in i_c corresponds to the power exchange between the dc link and the converter. However, if the circulating current is not controlled, it may also contain a number of harmonic components which are induced as a consequence of the capacitor voltage variations [14]. For the analysis, it may therefore be convenient to express the arm currents as

$$i_l = i_d + \sum_{h=1}^{\infty} \hat{i}_{hl}\cos(\omega_h t + \varphi_{hl}) \tag{3a}$$

$$i_u = i_d + \sum_{h=1}^{\infty} \hat{i}_{hu}\cos(\omega_h t + \varphi_{hu}) \tag{3b}$$

where i_d is the direct component, and $\hat{i}_{hl}$ and $\hat{i}_{hu}$ are the amplitudes of the harmonic components with the angular frequency ω_h. The angular frequency ω_h does not have to be an integer multiple of the fundamental frequency ω_1. This means that (3) can also be used to describe arm currents which are not periodic with the fundamental frequency.

The circulating current is directly related to the difference between the dc-link voltage and the sum of the inserted voltages in the arms [10], [13]. Accordingly

$$L\frac{di_c}{dt} = \frac{1}{2}v_d - \frac{v_l + v_u}{2} - Ri_c \tag{4}$$

where v_d is the dc-link voltage, v_l is the inserted voltage in the lower arm, and v_u is the inserted voltage in the upper arm. Assuming that the dc-link voltage is constant, this means that the harmonic content of i_c is determined by the sum of v_l and v_u.

If the converter has a bipolar dc link, i.e., the potentials at the dc-terminals are $\pm\frac{1}{2}v_d$, the potential at the ac terminal can be expressed as

$$v_s = v_l - \frac{1}{2}v_d + Ri_l + L\frac{di_l}{dt}. \tag{5}$$

Substituting i_l in (5) with (2a) yields

$$v_s = v_l - \frac{1}{2}v_d + Ri_c + L\frac{di_c}{dt} - \frac{1}{2}Ri_s - \frac{1}{2}L\frac{di_s}{dt}. \tag{6}$$

Combining (4) and (6) gives

$$v_s = \frac{1}{2}(v_l - v_u) - \frac{1}{2}Ri_s - \frac{1}{2}L\frac{di_s}{dt}. \tag{7}$$

Thus, it can be concluded that the alternating voltage is directly related to the difference between v_l and v_u.

III. Phase-Shifted Carrier Modulation

A detailed model of the M2C that is valid also at low switching frequencies must consider the switching state and capacitor voltage of each individual submodule. Therefore, in order to simplify the analysis, the N submodules in each arm will be referred to as submodule 1, 2, 3, ... , N. Furthermore, the switching function of submodule k is denoted s_k and is defined such that s_k is equal to 1 if submodule k is inserted, and equal to zero if submodule k is bypassed. By using phase-shifted carriers, each switching function s_k can be generated by comparing the reference waveform with a carrier waveform dedicated to submodule k [26]. This means that the harmonic content of s_k can be analyzed using conventional analysis methods for carrier-based modulation.

A. Carrier Harmonics and Sideband Harmonics

Assuming that double-edged modulation with natural sampling is used, the harmonic content of s_k can be described in terms of carrier harmonics and sideband harmonics [27]. Accordingly, the signal s_k can be expressed as

$$s_{kl} = \frac{1}{2} + \frac{m}{2}\cos(\omega_1 t) + \sum_{a=1}^{\infty}\sum_{b=-\infty}^{\infty} A_{abkl} \tag{8a}$$

$$s_{ku} = \frac{1}{2} - \frac{m}{2}\cos(\omega_1 t) + \sum_{a=1}^{\infty}\sum_{b=-\infty}^{\infty} A_{abku} \tag{8b}$$

where A_{abk} contains the carrier harmonics and sideband harmonics, and the indices l and u indicate upper and lower arm quantities, respectively. The components A_{abkl} and A_{abku} can be expressed analytically as [27]

$$A_{abkl} = \frac{2}{a\pi}J_b\Big(\frac{\pi a}{2}m\Big)\sin\Big[(a+b)\frac{\pi}{2}\Big] \cos[(a\omega_c + b\omega_1)t + a\theta_{kl}] \tag{9a}$$

$$A_{abku} = \frac{2}{a\pi}J_b\Big(\frac{\pi a}{2}m\Big)\sin\Big[(a+b)\frac{\pi}{2}\Big] \cos[(a\omega_c + b\omega_1)t + b\pi + a\theta_{ku}] \tag{9b}$$

where J_b are Bessel functions of the first kind, θ_k is the angular displacement of the kth carrier waveform, and ω_c is the angular frequency of the carrier waveform. The angular displacement θ_k can be expressed as

$$\theta_{kl} = \frac{2\pi}{N}k + \alpha \tag{10a}$$

$$\theta_{ku} = \theta_{kl} + \beta \tag{10b}$$

where α and β are arbitrary angular offsets which do not depend on the variable k. The angle α indicates the angular displacement between the reference waveform and the carrier waveforms, and the angle β indicates the angular displacement between the carrier waveforms in the upper and lower arms.

B. Properties of the Multilevel Waveform

The sums of all switching functions in the lower and upper arms are denoted s_l^{Σ} and s_u^{Σ}, respectively. That is, the signals s_l^{Σ} and s_u^{Σ} describe the normalized multilevel waveform which would ideally be inserted in each arm if the variations in the capacitor voltages are neglected. Accordingly

$$s_l^{\Sigma} = \sum_{k=1}^{N} s_{kl} \tag{11a}$$

$$s_u^{\Sigma} = \sum_{k=1}^{N} s_{ku}. \tag{11b}$$

Substituting s_k into (11) with (8) yields

$$s_l^{\Sigma} = N\left[\frac{1}{2} + \frac{m}{2}\cos(\omega_1 t) + s_{hl}\right] \tag{12a}$$

$$s_u^{\Sigma} = N\left[\frac{1}{2} - \frac{m}{2}\cos(\omega_1 t) + s_{hu}\right] \tag{12b}$$

where

$$s_{hl} = \frac{1}{N}\sum_{k=1}^{N}\sum_{a\in K_N}\sum_{b=-\infty}^{\infty} A_{abkl} \tag{13a}$$

$$s_{hu} = \frac{1}{N}\sum_{k=1}^{N}\sum_{a\in K_N}\sum_{b=-\infty}^{\infty} A_{abku} \tag{13b}$$

and

$$K_N = [N, 2N, 3N, \ldots]. \tag{14}$$

It is observed that the switching harmonics that do not cancel out in s_h are those for which the index a is a multiple of N. This means that the frequency of all carrier harmonics that appear in s_h will be multiples of N times the carrier frequency ω_c. The remaining harmonic content in s_h will then consist of the sidebands to the aforementioned carrier harmonics. This means that if $N\omega_c$ is a multiple of ω_1, all harmonics in s_h will be multiples of ω_1 as well. As a consequence, if $N\omega_c$ is an integer multiple of ω_1, the sum of the switching functions will not contain any subharmonics or other frequency components which are noninteger multiples of the fundamental frequency.

C. Displacement of Carrier Waveforms

As mentioned, the alternating voltage is determined by the difference between the upper and lower arm voltages. Consequently, switching harmonics in s_{hl} which are in phase with the corresponding switching harmonics in s_{hu} cancel out and will not appear in the alternating voltage. Similarly, switching harmonics that are in antiphase between the upper and lower arms cancel out when summed together and will therefore not appear on the dc side. As the phase angles of the switching harmonics are affected by the phase angle of the carrier waveforms this means that the angular displacements of the carrier waveforms can be chosen such that the harmonic performance is enhanced either on the dc side or on the ac side. These two different modulation strategies are referred to as (N+1)-level modulation and ($2N$+1)-level modulation, respectively.

1) (N+1)-Level Modulation: In order to minimize the harmonic distortion in the direct voltage, the displacement of the carrier waveforms should be chosen such that the switching harmonics are canceled out in the sum of s_{hl} and s_{hu}. This can be done by displacing the carrier waveforms in the upper arm by π rad from the carrier waveforms in the lower arm which gives that

$$\beta = \pi. \tag{15}$$

In this way, the upper and lower arm carrier harmonics in (9) will be in antiphase for odd values of a and the sideband harmonics will be in antiphase for even values of b. As a consequence, all switching harmonics in s_{hl} and s_{hu} will be in antiphase. Accordingly

$$s_{hu} = -s_{hl}. \tag{16}$$

In practice, this means that there will always be a constant number of submodules inserted in each phase leg. The case when β is chosen as in (15) is referred to as (N+1)-level modulation since this is the number of voltage levels that can be obtained at the ac terminal.

2) ($2N$+1)-Level Modulation: It is also possible to choose the displacement of the carrier harmonics in such a way that the harmonic performance of the alternating voltage is enhanced. This can be done by choosing the angular displacement β as

$$\beta = 0, \quad N \text{ is odd} \tag{17a}$$

$$\beta = \frac{\pi}{N}, \quad N \text{ is even.} \tag{17b}$$

Consequently, the first carrier harmonics and sideband harmonics which appear in s_{hl} will be in phase with the corresponding harmonics in s_{hu}. This means that the low-frequency harmonics will not appear in the alternating voltage. The harmonic components which are eliminated in the alternating voltage will, however, appear between the dc terminals. In practice, this means that the number of inserted submodules in each phase leg is not constant. As a consequence, there will be a common-mode voltage ripple across the upper and lower arm impedances which increases the effective number of levels from $N + 1$ to $2N + 1$ levels. Consequently, the case when β is chosen as (17) is referred to as ($2N$+1)-level modulation.

IV. Voltage Waveforms and Circulating Currents

The voltage waveforms do not only depend on the switching functions but are also directly dependent on the capacitor voltages. During the nominal operation of the converter, the submodule capacitors will be charged and discharged by the arm currents. The resulting voltage ripple must be taken into account in order to obtain a detailed model describing the inserted arm voltages, arm currents, and capacitor voltages.

A. Capacitor Voltages

The current flowing through the capacitor in submodule k is equal to the arm current if s_k is equal to unity. If s_k is equal to zero, the submodule is bypassed and no current is flowing through the capacitor. Consequently, the capacitor current in submodule k can be expressed as the product of s_k and the arm current. Accordingly

$$i_{\mathrm{cap},kl} = s_{kl} i_l \tag{18a}$$

$$i_{\mathrm{cap},ku} = s_{ku} i_u. \tag{18b}$$

The capacitor voltages are found by integrating the current flowing through the capacitor and dividing by the capacitance C. That is

$$v_{\mathrm{cap},kl} = V_{kl} + \frac{1}{C}\int s_{kl} i_l \, dt \tag{19a}$$

$$v_{\mathrm{cap},ku} = V_{ku} + \frac{1}{C}\int s_{ku} i_u \, dt \tag{19b}$$

where $v_{\mathrm{cap},k}$ is the voltage across the capacitor in submodule k of the corresponding arm and V_k is the initial value of $v_{\mathrm{cap},k}$. Substituting the arm currents i_l and i_u into (19) with (2) yields

$$v_{\mathrm{cap},kl} = V_{kl} + \frac{1}{C}\int \left(s_{kl} i_c - \frac{1}{2} s_{kl} i_s \right) dt \tag{20a}$$

$$v_{\mathrm{cap},ku} = V_{ku} + \frac{1}{C}\int \left(s_{ku} i_c + \frac{1}{2} s_{ku} i_s \right) dt. \tag{20b}$$

The integrals in (20) can be expressed as functions of the reference waveforms and switching harmonics by substituting

s_k with (8). Accordingly

$$v_{\mathrm{cap},kl} = V_{kl} + \frac{1}{C}\int\left[\left(\frac{1}{2} + \frac{m}{2}\cos(\omega_1 t) + \sum_{a=1}^{\infty}\sum_{b=-\infty}^{\infty} A_{abkl}\right) \times \left(i_c - \frac{1}{2}i_s\right)\right]dt \tag{21a}$$

$$v_{\mathrm{cap},ku} = V_{ku} + \frac{1}{C}\int\left[\left(\frac{1}{2} - \frac{m}{2}\cos(\omega_1 t) + \sum_{a=1}^{\infty}\sum_{b=-\infty}^{\infty} A_{abku}\right) \times \left(i_c + \frac{1}{2}i_s\right)\right]dt. \tag{21b}$$

Rearranging the equations yields

$$v_{\mathrm{cap},kl} = V_{kl} + v_{cal} + v_{cskl} \tag{22a}$$

$$v_{\mathrm{cap},ku} = V_{ku} + v_{cau} + v_{csku} \tag{22b}$$

where

$$v_{cal} = \frac{1}{C}\int\left(\frac{1}{2} + \frac{m}{2}\cos(\omega_1 t)\right)\left(i_c - \frac{1}{2}i_s\right)dt \tag{23a}$$

$$v_{cau} = \frac{1}{C}\int\left(\frac{1}{2} - \frac{m}{2}\cos(\omega_1 t)\right)\left(i_c + \frac{1}{2}i_s\right)dt \tag{23b}$$

and

$$v_{cskl} = \frac{1}{C}\int\left(\sum_{a=1}^{\infty}\sum_{b=-\infty}^{\infty} A_{abkl}\right)\left(i_c - \frac{1}{2}i_s\right)dt \tag{24a}$$

$$v_{csku} = \frac{1}{C}\int\left(\sum_{a=1}^{\infty}\sum_{b=-\infty}^{\infty} A_{abku}\right)\left(i_c + \frac{1}{2}i_s\right)dt. \tag{24b}$$

It is observed that the voltages v_{cal} and v_{cau} in (23) do not depend on the switching frequency or the index k. Hence, v_{ca} describes the voltage variations which are common for all submodules in each arm. These voltage variations are the same that would be achieved if the capacitor voltages were perfectly balanced within the arms. The individual voltage variations caused by the finite switching frequency are described by $v_{cs,k}$ in (24).

The multiplication of the modulating signal and the arm current in (21) will result in both direct and alternating components. When the alternating components are integrated over time they will result in a capacitor voltage ripple. However, the time integral of a direct component, i.e., a constant, will cause the value of the integral to approach infinity, or minus infinity if the constant is negative. Accordingly, in order for the capacitor voltages to be stable, the products in (21) must only result in alternating components. This means that all direct components, or constants, that are obtained from the multiplication of the terms in (21) must cancel out.

The integral in (21) can also be expressed as the sum of (23) and (24). The terms in (23) are the same for all submodules and do not depend on the index k. Accordingly, if the direct components should cancel out for all values of k, any direct components in (24) must be independent of the index k as well. Otherwise, it would be impossible for all direct components in the product in (21) to cancel out for all values of k.

The direct components in the products are obtained from the multiplication of two components with the same frequency. Since the arm current contains both a direct and fundamental frequency component this means that any direct or fundamental frequency component in A_{abk} can result in a net transfer of charge to the submodule. When two fundamental frequency components are multiplied, the time average of the product depends on the phase and amplitude of the two signals that are multiplied. Thus, in order to avoid diverging capacitor voltages any direct or fundamental frequency component in A_{abk} must be independent of the index k. However, in (9), it can be observed that if ω_c is an integer multiple of ω_1, there will be a sideband to the first carrier harmonic that is either a direct or fundamental frequency component. This sideband harmonic is affected by the index k and will therefore affect different submodules differently. Consequently, in order to avoid diverging capacitor voltages, the switching frequency should not be an integer multiple of the fundamental frequency.

It should be pointed out that at very low switching frequencies, there are additional frequencies which may cause the capacitor voltages to diverge. For example, if the switching frequency is 1.5 times the fundamental frequency, the second carrier harmonic will appear at three times the fundamental frequency. Hence, the third lower sideband to the second carrier harmonic will be at zero frequency and thus disturb the balancing of the capacitors. Therefore, a more stringent criterion would be that only the Nth multiple of the carrier frequency may be an integer multiple of the fundamental frequency.

B. Inserted Voltages

The voltage that is inserted by each submodule is given by the product of the switching function s_k and the capacitor voltage $v_{\mathrm{cap},k}$. Accordingly, the total voltage inserted in each arm can be expressed as

$$v_l = \sum_{k=1}^{N} s_{kl} v_{\mathrm{cap},kl} \tag{25a}$$

$$v_u = \sum_{k=1}^{N} s_{ku} v_{\mathrm{cap},ku} \tag{25b}$$

where v_l is the inserted voltage in the lower arm and v_u is the inserted voltage in the upper arm. Substituting $v_{\mathrm{cap},k}$ into (25) with (20) yields

$$v_l = \sum_{k=1}^{N} s_{kl}\left[V_{kl} + \frac{1}{C}\int\left(s_{kl}i_c - \frac{1}{2}s_{kl}i_s\right)dt\right] \tag{26a}$$

$$v_u = \sum_{k=1}^{N} s_{ku}\left[V_{ku} + \frac{1}{C}\int\left(s_{ku}i_c + \frac{1}{2}s_{ku}i_s\right)dt\right]. \tag{26b}$$

Accordingly

$$v_l = \sum_{k=1}^{N} s_{kl} V_{kl} + \frac{N}{C}\left[n_l \int n_l i_l \, dt + n_l \int s_{hl} i_l \, dt + s_{hl} \int n_l i_l \, dt + G_l \right] \quad (27a)$$

$$v_u = \sum_{k=1}^{N} s_{ku} V_{ku} + \frac{N}{C}\left[n_u \int n_u i_u \, dt + n_u \int s_{hu} i_u \, dt + s_{hu} \int n_u i_u \, dt + G_u \right] \quad (27b)$$

where n_l and n_u are given by (1), and the functions G_l and G_u are given by

$$G_l = \frac{1}{N} \sum_{k=1}^{N} \left[\left(\sum_{a=1}^{\infty} \sum_{b=-\infty}^{\infty} A_{abkl} \right) \times \left(\int \sum_{x=1}^{\infty} \sum_{y=-\infty}^{\infty} A_{xykl} i_l \, dt \right) \right] \quad (28a)$$

$$G_u = \frac{1}{N} \sum_{k=1}^{N} \left[\left(\sum_{a=1}^{\infty} \sum_{b=-\infty}^{\infty} A_{abku} \right) \times \left(\int \sum_{x=1}^{\infty} \sum_{y=-\infty}^{\infty} A_{xyku} i_u \, dt \right) \right] \quad (28b)$$

where the indices a and b have been replaced by x and y in the integrals such that the different terms can be identified when the products are expanded. It is observed that the interaction between the arm currents and the individual switching functions only affects the terms G_l and G_u in the arm voltages. The terms n_l and n_u in (27) are the normalized voltage references to the lower and upper arms, respectively, and the remaining terms, s_{hl} and s_{hu}, contains the switching harmonics of the ideal multilevel waveforms described in Section B.

Substituting the arm currents into (28) with (3), A_{abk} and A_{xyk} with (9), and evaluating the integrals yields

$$G_l = \frac{1}{4N} \sum_{k=1}^{N} \sum_{a=1}^{\infty} \sum_{y=-\infty}^{\infty} \sum_{x=1}^{\infty} \sum_{y=-\infty}^{\infty} \sum_{h=0}^{\infty} \times \left(\frac{\hat{A}_{abkl} \hat{A}_{xykl} \hat{i}_{hl} (f_{1,l} + f_{2,l})}{a\omega_c + b\omega_1 + \omega_h} + \frac{\hat{A}_{abkl} \hat{A}_{xykl} \hat{i}_{hl} (f_{3,l} + f_{4,l})}{a\omega_c + b\omega_1 - \omega_h} \right) \quad (29a)$$

$$G_u = \frac{1}{4N} \sum_{k=1}^{N} \sum_{a=1}^{\infty} \sum_{y=-\infty}^{\infty} \sum_{x=1}^{\infty} \sum_{y=-\infty}^{\infty} \sum_{h=0}^{\infty} \times \left(\frac{\hat{A}_{abku} \hat{A}_{xyku} \hat{i}_{hu} (f_{1,u} + f_{2,u})}{a\omega_c + b\omega_1 + \omega_h} + \frac{\hat{A}_{abku} \hat{A}_{xyku} \hat{i}_{hu} (f_{3,u} + f_{4,u})}{a\omega_c + b\omega_1 - \omega_h} \right) \quad (29b)$$

where $\hat{A}_{abk}$ and $\hat{A}_{xyk}$ are the amplitudes of the corresponding switching harmonics, and the functions f_1 through f_4 are given by

$$f_{1,l} = \sin[(\omega_{\rm sum} + \omega_h)t + \varphi_{hl} + \theta_{{\rm sum},l}] \quad (30a)$$

$$f_{2,l} = \sin[(\omega_{\rm dif} + \omega_h)t + \varphi_{hl} + \theta_{{\rm dif},l}] \quad (30b)$$

$$f_{3,l} = \sin[(\omega_{\rm sum} - \omega_h)t - \varphi_{hl} + \theta_{{\rm sum},l}] \quad (30c)$$

$$f_{4,l} = \sin[(\omega_{\rm dif} - \omega_h)t - \varphi_{hl} + \theta_{{\rm dif},l}] \quad (30d)$$

$$f_{1,u} = \sin[(\omega_{\rm sum} + \omega_h)t + \varphi_{hu} + \theta_{{\rm sum},u}] \quad (30e)$$

$$f_{2,u} = \sin[(\omega_{\rm dif} + \omega_h)t + \varphi_{hu} + \theta_{{\rm dif},u}] \quad (30f)$$

$$f_{3,u} = \sin[(\omega_{\rm sum} - \omega_h)t - \varphi_{hu} + \theta_{{\rm sum},u}] \quad (30g)$$

$$f_{4,u} = \sin[(\omega_{\rm dif} - \omega_h)t - \varphi_{hu} + \theta_{{\rm dif},u}] \quad (30h)$$

where

$$\omega_{\rm sum} = (a+x)\omega_c + (b+y)\omega_1 \quad (31a)$$

$$\omega_{\rm dif} = (a-x)\omega_c + (b-y)\omega_1 \quad (31b)$$

$$\theta_{{\rm sum},l} = (a+x)\theta_{kl} \quad (31c)$$

$$\theta_{{\rm dif},l} = (a-x)\theta_{kl} \quad (31d)$$

$$\theta_{{\rm sum},u} = (b+y)\pi + (a+x)\theta_{ku} \quad (31e)$$

$$\theta_{{\rm dif},u} = (b-y)\pi + (a-x)\theta_{ku}. \quad (31f)$$

By considering the definition of θ_{kl} and θ_{ku} in (10), it can be concluded that when (29) is summed over all values of k, the sinusoidal quantities in (30) will cancel out for all values of a and x except for those which $a \pm x$ is either zero or an integer multiple of N. This means that in all relevant cases, $\omega_{\rm sum}$ and $\omega_{\rm dif}$ are either zero, or integer multiples of $N\omega_c$. As a consequence, the frequencies which may appear in G_l and G_u are limited to integer multiples of $N\omega_c$ plus or minus ω_h. In practice, this means that if the arm current is periodic with the fundamental frequency period, and $N\omega_c$ is an integer multiple of ω_1, there will not be any subharmonics or noninteger multiples of the fundamental frequency in G_l or G_u.

As shown in the previous section, if $N\omega_c$ is an integer multiple of the fundamental frequency, the frequency of the harmonic components in s_h are multiples of ω_1. If the arm currents are periodic with the fundamental frequency period, this means that s_{hl}, s_{hu}, n_l, n_u, G_l, and G_u will all be periodic with the fundamental frequency period as well. This means that although there may be significant subharmonics in the capacitor voltages, they will not result in any subharmonics in the arm and line quantities.

C. Voltage Waveforms

By combining (27)–(28) and (2), the sum and difference of v_l and v_u can be expressed as it is observed that certain terms may cancel out, depending on the angular displacements of the carrier waveforms in the upper and lower arms. As an example,

if the carrier waveforms are in antiphase in the upper and lower arms, such that (15) is satisfied, each term that contains the sum of s_{hl} and s_{hu} will cancel out. This is, however, not the case if the angular displacement of the carrier waveforms is chosen such that (17) is satisfied. The two cases with $(N+1)$-level and $(2N+1)$-level modulation must therefore be considered separately.

1) (N+1)-Level Modulation: Given the assumption that the carrier waveforms in the upper and lower arms are displaced by π rad, the number of inserted submodules in each phase leg is always constant and a (N+1)-level waveform can be obtained at the ac terminal. The expression for the sum of v_l and v_u can then by simplified by substituting s_{hu} in (32) as shown at the bottom of the page with (16). Accordingly

$$\begin{aligned} v_l + v_u = &\sum_{k=1}^{N}(s_{kl}V_{kl} + s_{ku}V_{ku}) \\ &+ \frac{N}{C}\left[\frac{1}{2}\int\left(i_c - \frac{m}{2}i_s\cos(\omega_1 t)\right)dt\right. \\ &- N\frac{m}{2}\cos(\omega_1 t)\int\left(\frac{1}{2}i_s - mi_c\cos(\omega_1)\right)dt \\ &- \int\frac{1}{2}s_{hl}i_s\,dt + m\cos(\omega_1 t)\int s_{hl}i_c\,dt \\ &\left.- s_{hl}\int\left(\frac{1}{2}i_s - mi_c\cos(\omega_1 t)\right)dt + 2G_c\right]. \end{aligned} \tag{33}$$

where

$$\begin{aligned} G_c = \frac{1}{N}\sum_{k=1}^{N}&\left[\left(\sum_{a=1}^{\infty}\sum_{b=-\infty}^{\infty}A_{abkl}\right)\right. \\ &\left.\times\left(\int\sum_{a=1}^{\infty}\sum_{b=-\infty}^{\infty}A_{abkl}i_c\,dt\right)\right]. \end{aligned} \tag{34}$$

Similarly, the difference between the inserted voltages can be simplified to

$$\begin{aligned} v_l - v_u = &\sum_{k=1}^{N}(s_{kl}V_{kl} - s_{ku}V_{ku}) \\ &+ \frac{N}{C}\left[-\frac{1}{2}\int\left(\frac{1}{2}i_s - mi_c\cos(\omega_1 t)\,dt\right)\right. \\ &+ N\frac{m}{2}\cos(\omega_1 t)\int\left(i_c - \frac{m}{2}i_s\cos(\omega_1 t)\right)dt \\ &+ \int s_{hl}i_c\,dt - m\cos(\omega_1 t)\int\frac{1}{2}s_{hl}i_s\,dt \\ &\left.+ s_{hl}\int\left(i_c - \frac{m}{2}i_s\cos(\omega_1 t)\right)dt - 2G_s\right] \end{aligned} \tag{35}$$

where

$$\begin{aligned} G_s = \frac{1}{N}\sum_{k=1}^{N}&\left[\left(\sum_{a=1}^{\infty}\sum_{b=-\infty}^{\infty}A_{abkl}\right)\right. \\ &\left.\times\left(\frac{1}{2}\int\sum_{a=1}^{\infty}\sum_{b=-\infty}^{\infty}A_{abkl}i_s\,dt\right)\right]. \end{aligned} \tag{36}$$

The circulating current and alternating voltage can be described by combining (33) with (4) and (35) with (7). It is concluded that the dynamic system governing the arm and line quantities is time-variant. This means that a certain harmonic component in i_c or i_s can generate harmonic components of other frequencies in (33) and (35). Although it is difficult to obtain an explicit solution to the dynamic equations, it is possible to determine which harmonic components that may or may not appear in the arm and line quantities.

If there are only odd-order harmonics in the alternating current, it can be shown that for certain switching frequencies there will not be any odd-order harmonics or subharmonics in the circulating current. In order to show this, it assumed that the

$$\begin{aligned} v_l + v_u = &\sum_{k=1}^{N}(s_{kl}V_{kl} + s_{ku}V_{ku}) + \frac{N}{C}\left[\frac{1}{2}\int\left(i_c - \frac{m}{2}i_s\cos(\omega_1 t)\right)dt - \frac{m}{2}\cos(\omega_1 t)\int\left(\frac{1}{2}i_s - mi_c\cos(\omega_1)\right)dt\right. \\ &+ \frac{1}{2}\int\left((s_{hl}+s_{hu})i_c - \frac{1}{2}(s_{hl}-s_{hu})i_s\right)dt + \frac{m}{2}\cos(\omega_1 t)\int\left((s_{hl}-s_{hu})i_c - \frac{1}{2}(s_{hl}+s_{hu})i_s\right)dt \\ &\left.+ (s_{hl}+s_{hu})\int\left(\frac{1}{2}i_c - \frac{m}{4}i_s\cos(\omega_1 t)\right)dt - (s_{hl}-s_{hu})\int\left(\frac{1}{4}i_s - \frac{m}{2}i_c\cos(\omega_1)\right)dt + G_l + G_u\right] \end{aligned} \tag{32a}$$

$$\begin{aligned} v_l - v_u = &\sum_{k=1}^{N}(s_{kl}V_{kl} - s_{ku}V_{ku}) + \frac{N}{C}\left[-\frac{1}{2}\int\left(\frac{1}{2}i_s - mi_c\cos(\omega_1)\right)dt + \frac{m}{2}\cos(\omega_1 t)\int\left(i_c - \frac{m}{2}i_s\cos(\omega_1 t)\right)dt\right. \\ &+ \frac{1}{2}\int\left((s_{hl}-s_{hu})i_c - \frac{1}{2}(s_{hl}+s_{hu})i_s\right)dt + \frac{m}{2}\cos(\omega_1 t)\int\left((s_{hl}+s_{hu})i_c - \frac{1}{2}(s_{hl}-s_{hu})i_s\right)dt \\ &\left.+ (s_{hl}-s_{hu})\int\left(\frac{1}{2}i_c - \frac{m}{4}i_s\cos(\omega_1 t)\right)dt - (s_{hl}+s_{hu})\int\left(\frac{1}{4}i_s - \frac{m}{2}i_c\cos(\omega_1)\right)dt + G_l - G_u\right] \end{aligned} \tag{32b}$$

switching frequency is chosen such that $N\omega_c$ is an odd multiple of ω_1 if N is odd, or an even multiple of N if N is even. As shown, this means that s_{hl} and s_{hu} only contain odd-order harmonics. It is also assumed that the initial values of V_k of the capacitor voltages are such that

$$\sum_{k=1}^{N}(s_{kl}V_{kl}+s_{ku}V_{ku})=v_d \tag{37}$$

is satisfied. The dynamics of the circulating current can then be expressed by substituting the sum of v_l and v_u into (4) with (33) and applying (37). Accordingly

$$\begin{aligned}2Ri_c+2L\frac{di_c}{dt}=\frac{N}{C}\Bigg[&\frac{1}{2}\int\left(i_c-\frac{m}{2}i_s\cos(\omega_1 t)\right)\,dt\\&-N\frac{m}{2}\cos(\omega_1 t)\int\left(\frac{1}{2}i_s-mi_c\cos(\omega_1 t)\right)\,dt\\&-\int\frac{1}{2}s_{hl}i_s\,dt+m\cos(\omega_1 t)\int s_{hl}i_c\,dt\\&-s_{hl}\int\left(\frac{1}{2}i_s-mi_c\cos(\omega_1 t)\right)\,dt+2G_c\Bigg].\end{aligned} \tag{38}$$

It is observed that all terms containing the circulating current are multiplied with either a direct component or the product of two odd-order harmonics. This means that all odd-order harmonics or subharmonics in the circulating current will only result in odd-order harmonics or subharmonics in (38). It is also observed that the alternating current i_s in (38) is always multiplied with a fundamental-frequency component or odd-order harmonic. This means that if i_s only contains odd-order harmonics, these products will only result in even-order harmonics in (38). It is concluded that the dynamics of the even-order harmonics are decoupled from the dynamics governing the odd-order harmonics and subharmonics. Therefore, the circulating current is subdivided into two terms

$$i_c=i_{ce}+i_{cso} \tag{39}$$

where i_{ce} contains the direct component and all even-order harmonics, and i_{cso} contains all odd-order harmonics and subharmonics. The dynamic equation describing the even-order harmonics is then given by

$$\begin{aligned}2Ri_{ce}+2L\frac{di_{ce}}{dt}=\frac{N}{C}\Bigg[&\frac{1}{2}\int\left(i_{ce}-\frac{m}{2}i_s\cos(\omega_1 t)\right)\,dt\\&-\frac{m}{2}\cos(\omega_1 t)\int\left(\frac{1}{2}i_s-mi_{ce}\cos(\omega_1)\right)\,dt\\&-\int\frac{1}{2}s_{hl}i_s\,dt+m\cos(\omega_1 t)\int s_{hl}i_{ce}\,dt\\&-s_{hl}\int\left(\frac{1}{2}i_s-mi_{ce}\cos(\omega_1 t)\right)\,dt+2G_{ce}\Bigg]\end{aligned} \tag{40}$$

where

$$\begin{aligned}G_{ce}=\frac{1}{N}\sum_{k=1}^{N}\Bigg[&\left(\sum_{a=1}^{\infty}\sum_{b=-\infty}^{\infty}A_{abkl}\right)\\&\times\left(\int\sum_{a=1}^{\infty}\sum_{b=-\infty}^{\infty}A_{abkl}i_{ce}\,dt\right)\Bigg]\end{aligned} \tag{41}$$

assuming that the current i_s only contains odd-order harmonics. Similarly, the dynamics of the subharmonics and odd-order harmonics are given by

$$\begin{aligned}2Ri_{cso}+2L\frac{di_{cso}}{dt}=\frac{1}{2C}\Bigg[&N\frac{1}{2}\int i_{cso}\,dt\\&+N\frac{m}{2}\cos(\omega_1 t)\int mi_{cso}\cos(\omega_1)\,dt\\&+m\cos(\omega_1 t)\int s_{hl}i_{cso}\,dt\\&+s_{hl}\int i_{cso}m\cos(\omega_1 t)\,dt+2G_{cso}\Bigg]\end{aligned} \tag{42}$$

where

$$\begin{aligned}G_{cso}=\frac{1}{N}\sum_{k=1}^{N}\Bigg[&\left(\sum_{a=1}^{\infty}\sum_{b=-\infty}^{\infty}A_{abkl}\right)\\&\times\left(\int\sum_{a=1}^{\infty}\sum_{b=-\infty}^{\infty}A_{abkl}i_{cso}\,dt\right)\Bigg].\end{aligned} \tag{43}$$

Multiplying both sides of (42) with i_{cso} and solving for Ri_{cso}^2 yields

$$\begin{aligned}Ri_{cso}^2=&-Li_{cso}\frac{di_{cso}}{dt}-\frac{1}{2C}\Bigg[N\frac{1}{2}i_{cso}\int i_{cso}\,dt\\&+N\frac{m}{2}i_{cso}\cos(\omega_1 t)\int mi_{cso}\cos(\omega_1)\,dt\\&+i_{cso}m\cos(\omega_1 t)\int s_{hl}i_{cso}\,dt\\&+s_{hl}i_{cso}\int i_{cso}m\cos(\omega_1 t)\,dt+2i_{cso}G_{cso}\Bigg].\end{aligned} \tag{44}$$

The product $i_{cso}G_{cso}$ can also be expressed as

$$\begin{aligned}i_{cso}G_{cso}=\frac{1}{N}\sum_{k=1}^{N}\Bigg[&\left(s_{hl}i_{cso}+\sum_{a\notin K_N}^{\infty}\sum_{b=-\infty}^{\infty}A_{abkl}i_{cso}\right)\\&\left(\int s_{hl}i_{cso}+\sum_{a\notin K_N}^{\infty}\sum_{b=-\infty}^{\infty}A_{abkl}i_{cso}\,dt\right)\Bigg].\end{aligned} \tag{45}$$

That is

$$i_{cso}G_{cso} = \frac{1}{N}\sum_{k=1}^{N}\Bigg[\Bigg(s_{hl}i_{cso}\int s_{hl}i_{cso}\,dt + \sum_{a\notin K_N}^{\infty}\sum_{b=-\infty}^{\infty}A_{abkl}i_{cso} \int\sum_{a\notin K_N}^{\infty}\sum_{b=-\infty}^{\infty}A_{abkl}i_{cso}\,dt\Bigg) + \sum_{a\notin K_N}^{\infty}\sum_{b=-\infty}^{\infty}A_{abkl}i_{cso}\int s_{hl}i_{cso},dt + s_{hl}i_{cso}\int\sum_{x\notin K_N}^{\infty}\sum_{b=-\infty}^{\infty}A_{abkl}i_{cso}\,dt\Bigg] \quad (46)$$

which can also be expressed as

$$i_{cso}G_{cso} = \frac{1}{N}\sum_{k=1}^{N}\Bigg[\Bigg(s_{hl}i_{cso}\int s_{hl}i_{cso}\,dt + \sum_{a\notin K_N}^{\infty}\sum_{b=-\infty}^{\infty}A_{abkl}i_{cso}\int\sum_{a\notin K_N}^{\infty}\sum_{b=-\infty}^{\infty}A_{abkl}i_{cso}\,dt\Bigg) + \frac{d}{dt}\Bigg[\Bigg(\int s_{hl}i_{cso},dt\Bigg)\Bigg(\int\sum_{a\notin K_N}^{\infty}\sum_{b=-\infty}^{\infty}A_{abkl}i_{cso}\,dt\Bigg)\Bigg]. \quad (47)$$

When summed over all values of k, the last term containing A_{abk} becomes zero. The expression for $i_{cso}G_{cso}$ can then be simplified

$$i_{cso}G_{cso} = \frac{1}{N}\sum_{k=1}^{N}\Bigg[\Bigg(s_{hl}i_{cso}\int s_{hl}i_{cso}\,dt + \sum_{a\notin K_N}^{\infty}\sum_{b=-\infty}^{\infty}A_{abkl}i_{cso}\int\sum_{a\notin K_N}^{\infty}\sum_{b=-\infty}^{\infty}A_{abkl}i_{cso}\,dt\Bigg)\Bigg]. \quad (48)$$

Substituting $i_{cso}G_{cso}$ into (49) with (48) yields

$$Ri_{cso}^2 = -Li_{cso}\frac{di_{cso}}{dt} - \frac{N}{2C}\Bigg[\frac{1}{2}i_{cso}\int i_{cso}\,dt + \frac{m}{2}i_{cso}\cos(\omega_1 t)\int mi_{cso}\cos(\omega_1)\,dt + i_{cso}m\cos(\omega_1 t)\int s_{hl}i_{cso}\,dt + s_{hl}i_{cso}\int i_{cso}m\cos(\omega_1 t)\,dt + 2s_{hl}i_{cso}\int s_{hl}i_{cso}\,dt + 2\frac{1}{N}\sum_{k=1}^{N}\Bigg[\sum_{a\notin K_N}^{\infty}\sum_{b=-\infty}^{\infty}A_{abkl}i_{cso} \int\sum_{a\notin K_N}^{\infty}\sum_{b=-\infty}^{\infty}A_{abkl}i_{cso}\,dt\Bigg] \quad (49)$$

which can be expressed as

$$Ri_{cso}^2 = -Li_{cso}\frac{di_{cso}}{dt} - \frac{N}{2C}\Bigg[\frac{1}{2}i_{cso}\int i_{cso}\,dt + \Bigg(\frac{m}{\sqrt{2}}i_{cso}\cos(\omega_1 t) + \sqrt{2}i_{cso}s_{hl}\Bigg)\int\Bigg(\frac{m}{\sqrt{2}}i_{cso}\cos(\omega_1 t) + \sqrt{2}i_{cso}s_{hl}\Bigg)dt + 2\frac{1}{N}\sum_{k=1}^{N}\Bigg[\sum_{a\notin K_N}^{\infty}\sum_{b=-\infty}^{\infty}A_{abkl}i_{cso}\int\sum_{a\notin K_N}^{\infty}\sum_{b=-\infty}^{\infty}A_{abkl}i_{cso}\,dt\Bigg]. \quad (50)$$

It is observed that all integrals in (50) are in the form

$$f(t)\int f(t)\,dt. \quad (51)$$

In order for the system to be stable, the right-hand side of (50) cannot have a direct component. However, if the system is unstable in such way that the time-average of the right-hand side of (50) is not zero, the time average would always be positive. The reason for this is that since all terms in (50) are in the form (51), if the time-average of the integral is negative, then the direct component of $f(t)$ in (51) is negative as well, which results in a positive product. Therefore, it can be concluded that the right-hand side of the dynamic equation for i_{cso} cannot have a positive direct component which means that the only valid solution is $i_{cso} = 0$. Consequently, it can be concluded that any odd-order harmonics or subharmonics in the circulating current will appear as damped oscillations. It can also be shown that an even-order harmonic in i_c, or an odd-order harmonic in i_s, will only generate odd-order harmonics in the difference of the arm voltages $v_l - v_u$. Accordingly, it can be concluded that if $N\omega_c$ is an odd multiple of ω_1 when N is odd, or an even multiple of ω_1 when N is even, the dc-side quantities will only contain even-order harmonics whereas the ac-side quantities will only contain odd-order harmonics when (N+1)-level modulation is used.

There is advantage in choosing the carrier frequency such that the circulating current only contains even-order harmonics and the alternating voltage only contains odd-order harmonics. The reason for this is that the direct and fundamental frequency components can be considered to be even and odd-order harmonics, respectively. This can cause unbalanced operating conditions in the upper and lower arms, since a fundamental frequency component in the circulating current would cause the alternating current through the upper arm to be different from the alternating current through the lower arm. Similarly, a direct component in the alternating voltage means that the direct component of the arm voltages are different in the upper and lower arms.

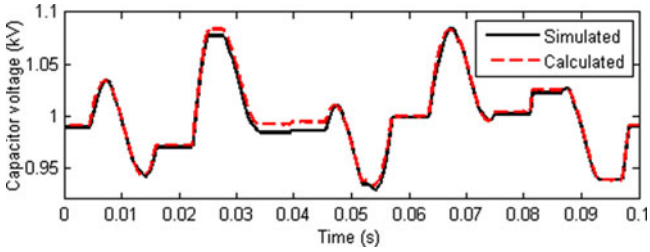

Fig. 2. Calculated and simulated capacitor voltages at 130-Hz switching frequency.

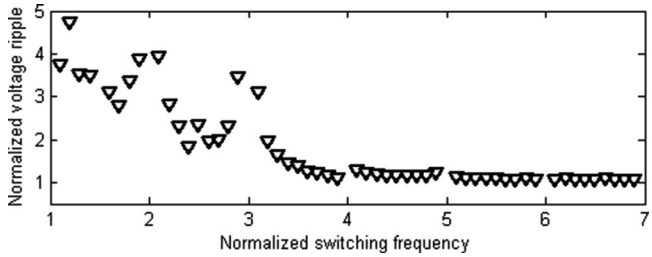

Fig. 3. Normalized capacitor voltage ripple with an 8° inductive power angle and modulation index 1.0 as a function of the switching frequency.

2) (2N+1)-Level Modulation: In the case, when the displacements of the carrier waveforms are chosen such that (2N+1) voltage levels are obtained, the sum of s_{hl} and s_{hu} do not always cancel out and the difference $s_{hl} - s_{hu}$ is not always equal to $2s_{hl}$. This means that (32) cannot be simplified in the way as for (N+1)-level modulation. Consequently, the expressions for the sum and difference of the arm voltages become more complex and difficult to overlook. It is, however, still possible to identify which harmonic components will be generated in the arm and line quantities.

According to (13), the harmonic components which appear in s_{hl} and s_{hu} are the carrier harmonics and sidebands to carrier multiples of N. By combining (9) and (17), it can also be concluded that the harmonic components in s_{hl} and s_{hu} are in phase when the carrier multiple a is an odd multiple of N. Similarly, the harmonic components in s_{hl} and s_{hu} can be shown to be in antiphase when the carrier multiple a is an even multiple of N.

In order to separate odd- and even-order harmonics, the carrier frequency should be chosen such that the sum of s_{hl} and s_{hu} only contains even-order harmonics and the difference $s_{hl} - s_{hu}$ only contains odd-order harmonics. This occurs when $N\omega_c$ is an even multiple of ω_1 when N is odd, or an odd multiple of ω_1 when N is even. In this way, the dc-side quantities will only contain even-order harmonics whereas the ac-side quantities will only contain odd-order harmonics when (2N+1)-level modulation is used. Such a separation of the odd- and even-order harmonics is desirable since it will yield balanced operating conditions in the upper and lower arms.

D. Switching Frequency and Capacitor Voltage Ripple

It is known that there is a tradeoff between the capacitor voltage ripple and the switching frequency [16]. With the presented analysis, the capacitor voltage ripple can be expressed as a function of the arm currents for any given switching frequency. However, the harmonic distortion in the output waveforms is fairly low in high-voltage applications where the number of submodules per arm is large [16]. Furthermore, the low-frequency harmonics that are induced in the circulating current by the capacitor voltage variations can be eliminated by implementing a main circuit filter as described in [24]. Accordingly, for a qualitative investigation of the relation between the switching frequency and capacitor voltage ripple it can be assumed that the circulating current i_c is a direct current and the ac-side current i_s is a pure sinusoid.

TABLE I
SIMULATION PARAMETERS AND EXPERIMENTAL SETUP

	Simulations	Experimental setup
Number of submodules N	5 per arm	5 per arm
DC-link voltage v_d	5 kV	500 V
Modulation index m	1.0	0.95
Arm inductance L	20 mH	14 mH
Submodule capacitance C	730 μF	730 μF
Switching frequency	120–200 Hz	110 Hz
Voltage levels	2N+1	N+1 and 2N+1
Load	Passive	Passive

In order to validate that reasonable values are obtained even if it is assumed that the arm currents contain a pure sinusoid with a dc-offset, the calculated capacitor voltages can be compared with simulation results. In Fig. 2, simulation results from an M2C using a main circuit filter as described in [24] are compared with the analytical expressions. It is observed that although the analytical expression is based on certain approximations, a satisfactory agreement is obtained with the simulated values. Thus, it can be concluded that the approximation can be used for a qualitative description of the capacitor voltage ripple.

As indicated by (21), the capacitor voltage ripple is not directly related to the number of submodules per arm. The angular displacement of the carrier waveform will, however, have an impact on the capacitor voltage ripple. Therefore, in order to clearly illustrate the relation between the switching frequency and the capacitor voltage ripple, the peak-to-peak capacitor voltage ripple is calculated for all possible angular displacements of the carrier waveforms, in steps of 1°. The maximum capacitor voltage ripple is then noted for each frequency. The normalized peak-to-peak capacitor voltage ripples at unity modulation index are presented in Fig. 3 as a function of the switching frequency. The switching frequency in Fig. 3 has been normalized with respect to the fundamental frequency and the capacitor voltage ripple is normalized with respect to the capacitor voltage ripple in (23) that would be obtained with an infinite switching frequency. It should be made clear that the voltage ripples in Fig. 3 were calculated without any feedback control for balancing the capacitor voltages. Thus, the presented values indicate how the switching harmonics and arm currents interact and generate additional harmonic components in the capacitor voltages. It can be observed that for low switching frequencies, e.g., below twice

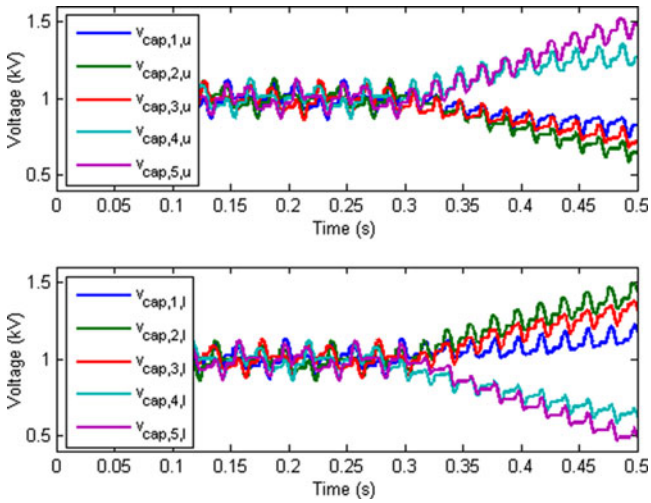

Fig. 4. Simulated capacitor voltages when the switching frequency is increased from 120 to 150 Hz at 0.3 s.

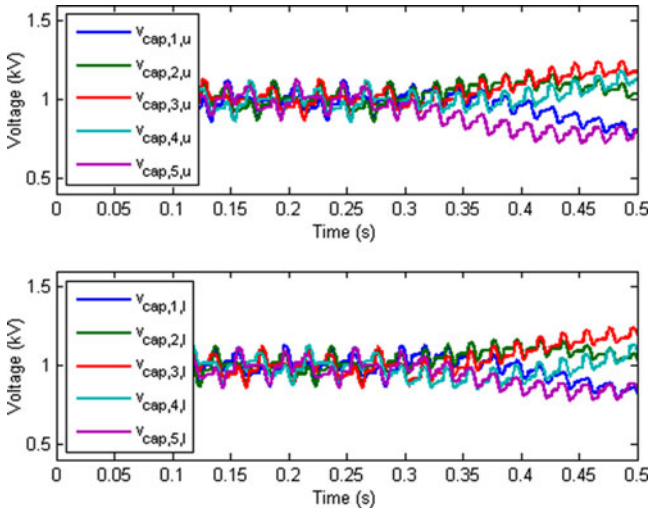

Fig. 5. Simulated capacitor voltages when the switching frequency is increased from 120 to 200 Hz at 0.3 s.

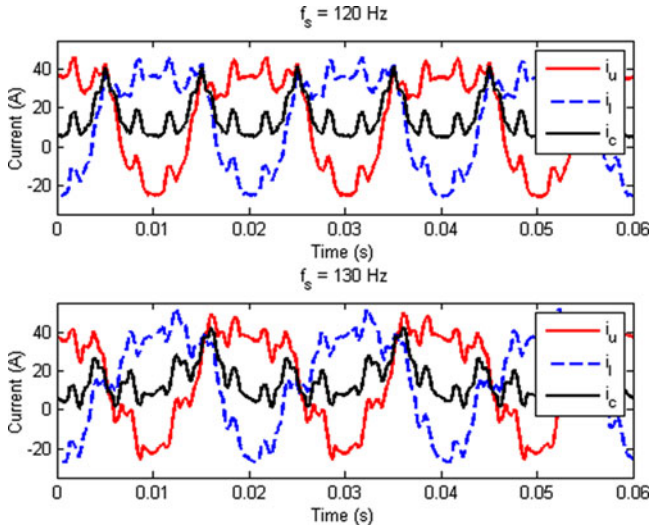

Fig. 6. Simulated arm currents and circulating currents with 120-Hz (upper) and 130-Hz (lower) switching frequency.

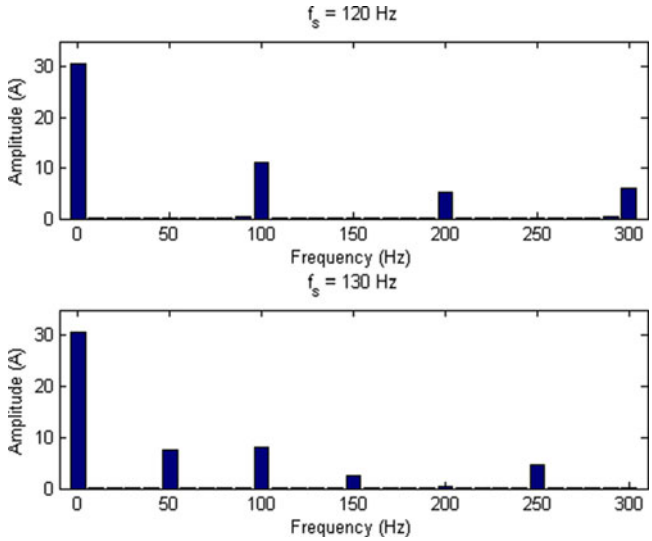

Fig. 7. Ampltiudes of the harmonic components in the circulating current at 120-Hz (upper) and 130-Hz (lower) switching frequency.

the fundamental frequency, these additional harmonics cause a significant increase in the peak-to-peak capacitor voltage ripple.

V. Simulations and Experimental Results

The theoretical findings are validated by both simulations and experimental results. The specifications of the simulated system and the experimental setup are shown in Table 1.

A. Simulation Results

The simulated system has five submodules per arm, which means that the carrier waveforms should be shifted by π over 5 rad between the upper and lower arms. The carrier waveforms are distributed such that the upper arm carriers are in phase with the lower arm carriers. This means that the resulting number of levels will be $(2N+1)$. Consequently, the product of the carrier frequency and the number of submodules should be an even multiple of the fundamental frequency in order to obtain balanced operating conditions.

The aim of the first simulation is to demonstrate the importance of avoiding switching frequencies which are integer multiples of the fundamental frequency. In the first simulation, the switching frequency is initially set to 120 Hz, at 0.3 s the switching frequency is increased to 150 Hz. The simulated capacitor voltages are shown in Fig. 4. It is observed that the capacitor voltages are, in-deed, balanced when the switching frequency is 120 Hz. However, after 0.3 s, the capacitor voltages start to diverge as the switching frequency was increased to 150 Hz which is an integer multiple of the 50-Hz fundamental frequency. This was expected since the frequency of one of the sidebands to the first carrier multiple coincides with the fundamental frequency.

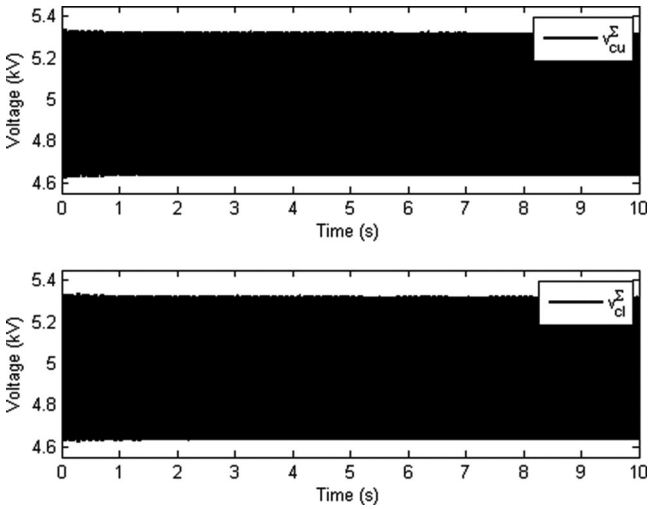

Fig. 8. Sum of the upper and lower arm capacitor voltages at 120-Hz switching frequency.

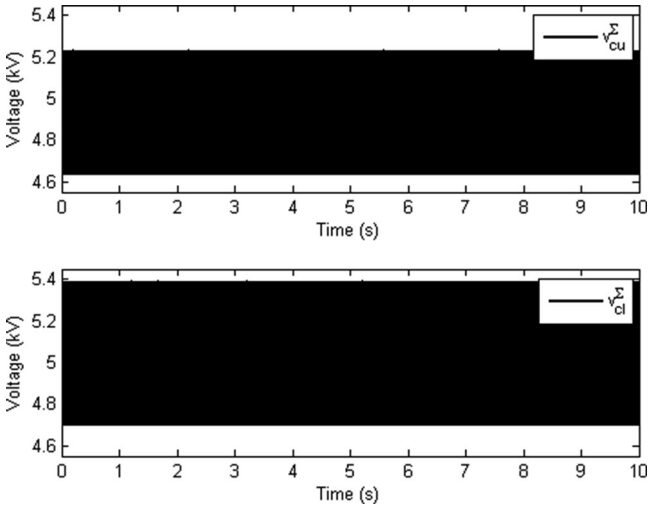

Fig. 9. Sum of the upper and lower arm capacitor voltages at 130-Hz switching frequency.

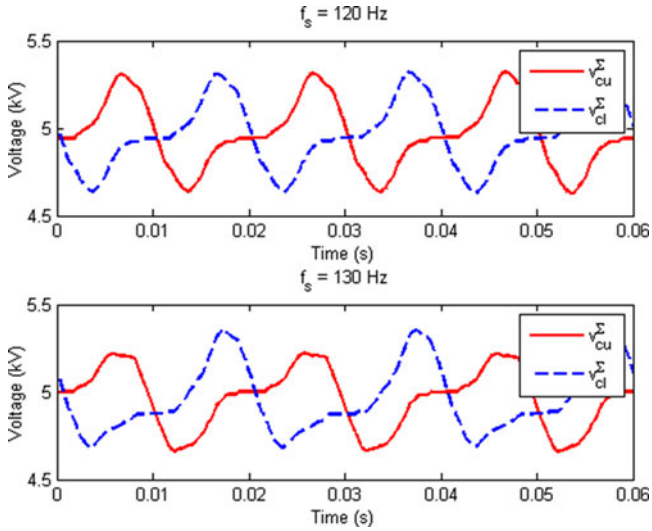

Fig. 10. Sum of the upper and lower arm capacitor voltages at 120-Hz (upper) and 130-Hz (lower) switching frequency.

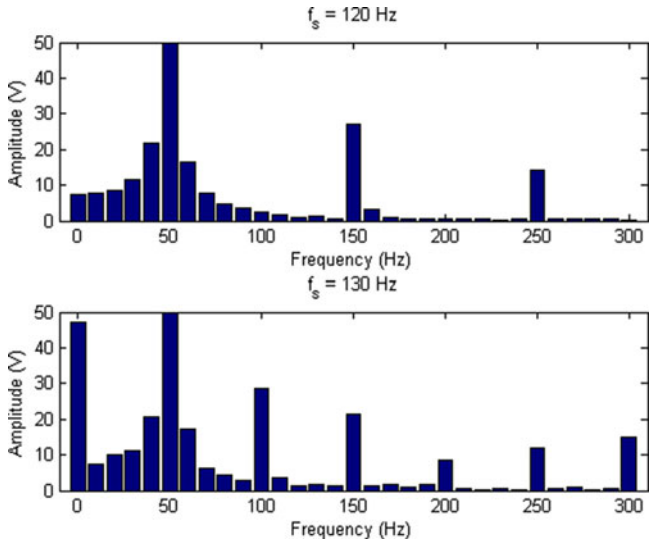

Fig. 11. Amplitudes of the harmonic components in the alternating voltage at 120-Hz (upper) and 130-Hz (lower) switching frequency. The amplitude of the 50-Hz component is in both cases 2.47 kV.

It can be demonstrated that the capacitor voltages become unbalanced also if the switching frequency is changed from 120 to 200 Hz, which is the next multiple of the fundamental frequency after 150 Hz. The simulation results for this case are shown in Fig. 5. As expected, the capacitor voltages start to diverge as the switching frequency is changed at 0.3 s. This is a consequence of the fact that the frequency of one of the sidebands to the first carrier multiple is zero. The effect is, however, less dramatic compared to the previous case. The reason for this is that in this case it is the fourth lower sideband to the first carrier harmonic that disturbs the balancing of the capacitor voltages. In the previous case, when the switching frequency was 150 Hz, it was the second lower sideband, which has a much larger amplitude that caused the disturbance.

The theoretical results indicate that there will be odd-order harmonics in the circulating current if the product of the number of submodules per arm and the switching frequency is not an even multiple of the fundamental frequency. In order to validate the theoretical results, the system is simulated with 120-Hz switching frequency which gives an even multiple of the fundamental frequency, and also 130-Hz switching frequency which results in an odd multiple of the fundamental frequency. The simulated arm currents and the circulating current are shown in Fig. 6. It is observed that the upper and lower arm waveforms are similar at the 120-Hz switching frequency but not for the 130-Hz switching frequency.

The difference between the current waveforms in Fig. 6 can be explained by the fact that the odd- and even-order harmonics are separated between the dc- and ac-sides at 120-Hz switching frequency, but not at 130-Hz switching frequency. This can be

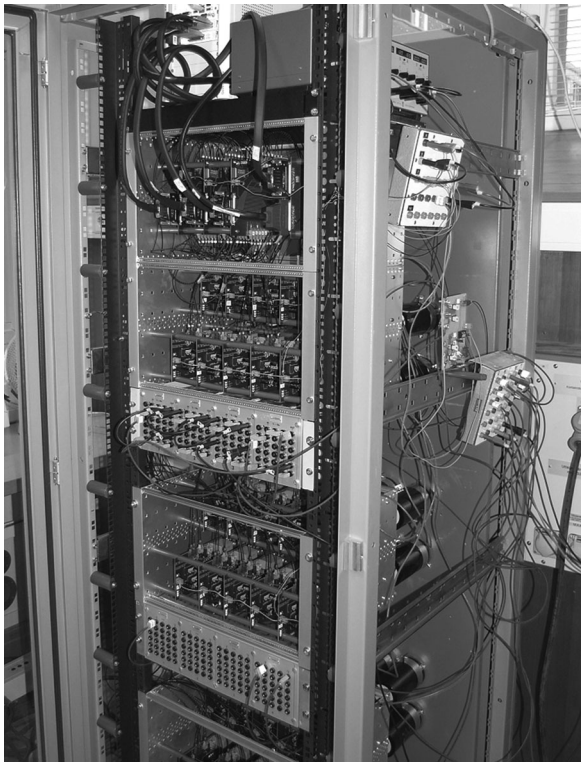

Fig. 12. A down-scaled laboratory prototype of the M2C.

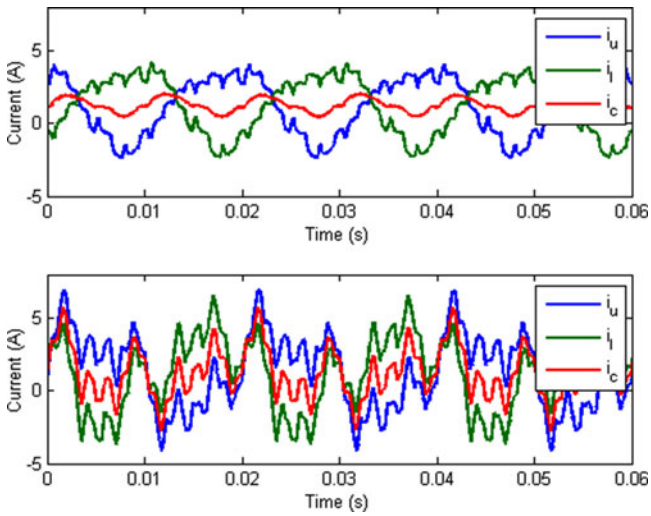

Fig. 13. Measured arm currents with $(N+1)$-level modulation (upper) and $(2N+1)$-level modulation (lower).

verified by taking the discrete Fourier transform (DFT) of the simulated waveforms. The amplitudes of the harmonic components are shown in Fig. 7. It is observed that the circulating current contains only even-order harmonics at the 120-Hz switching frequency, whereas it contains both odd and even-order harmonics at 130-Hz switching frequency.

The difference in the upper- and lower-arm waveforms at 130-Hz switching frequency also affects the capacitor voltages. The sum of the capacitor voltages in the lower arm v_{cl}^{Σ} and the

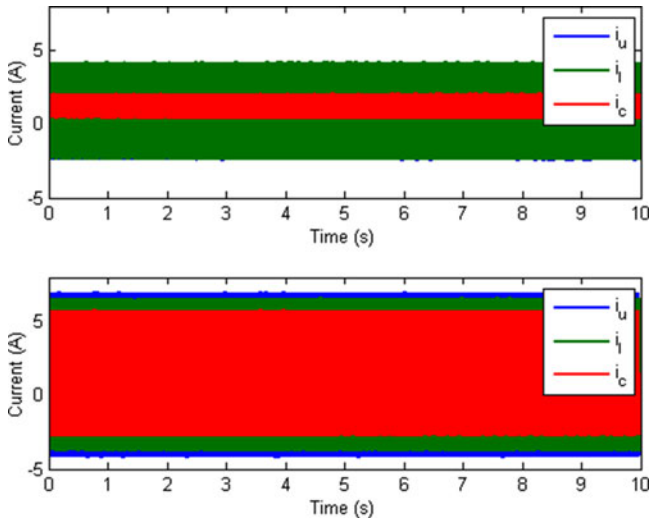

Fig. 14. Measured arm currents with $(N+1)$-level modulation (upper) and $(2N+1)$-level modulation (lower).

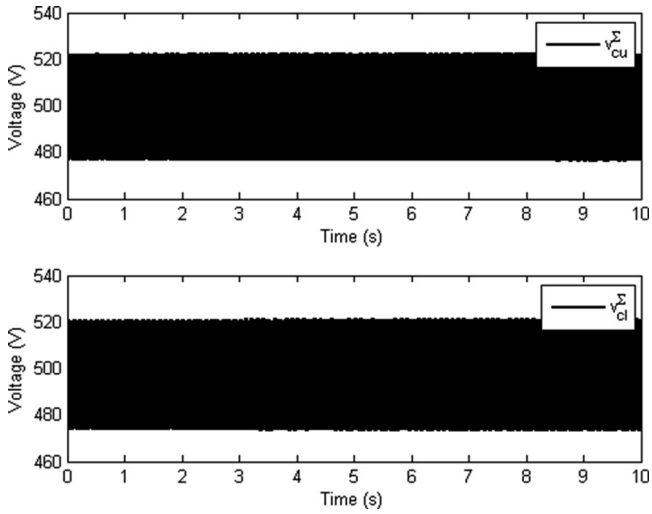

Fig. 15. Sum of the measured capacitor voltages in the upper (upper) and lower (lower) arms at $(N+1)$-level modulation.

sum of the capacitor voltages in the upper arm v_{cu}^{Σ} are shown in Fig. 8 for 120-Hz switching frequency and in Fig. 9 for 130-Hz switching frequency. It is observed that the capacitor voltages are stable in both cases. However, at 130-Hz switching frequency, there is a clear difference between the upper and lower arm capacitor voltages. A more detailed view of v_{cu}^{Σ} and v_{cl}^{Σ} for the two cases is given in Fig. 10. It is observed that the capacitor voltages are similar, but phase-shifted, at 120-Hz switching frequency. However, when the switching frequency is increased to 130 Hz, there is a clear difference in the shape of the capacitor voltage waveforms in the upper and lower arms.

The theoretical findings also indicate that there should only be odd-order harmonics in the alternating voltage when the switching frequency is 120 Hz. This is verified by taking the DFT of the simulated ac-terminal voltage. The amplitudes of the harmonic components in the alternating voltage are shown in Fig. 11. It is

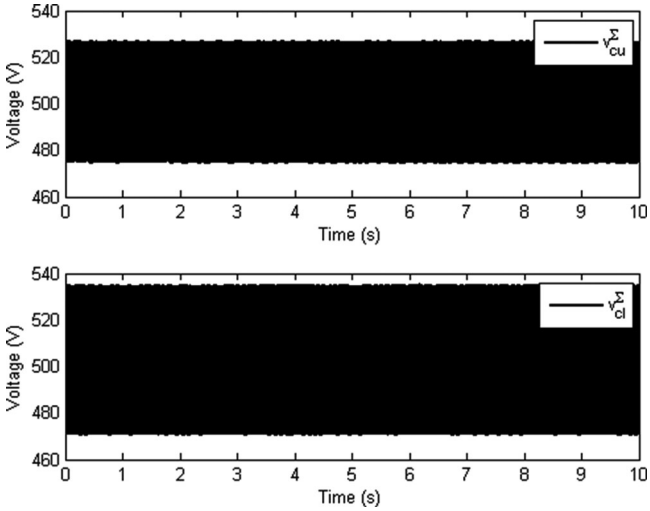

Fig. 16. Sum of the measured capacitor voltages in the upper (upper) and lower (lower) arms at $(2N+1)$-level modulation.

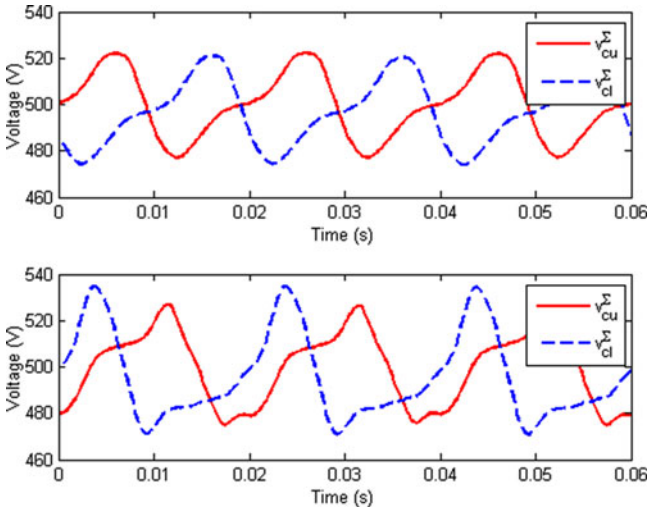

Fig. 17. Sum of the measured capacitor voltages in the upper (red) and lower (blue) arms at $(N+1)$-level (upper) and $(2N+1)$-level (lower) modulation.

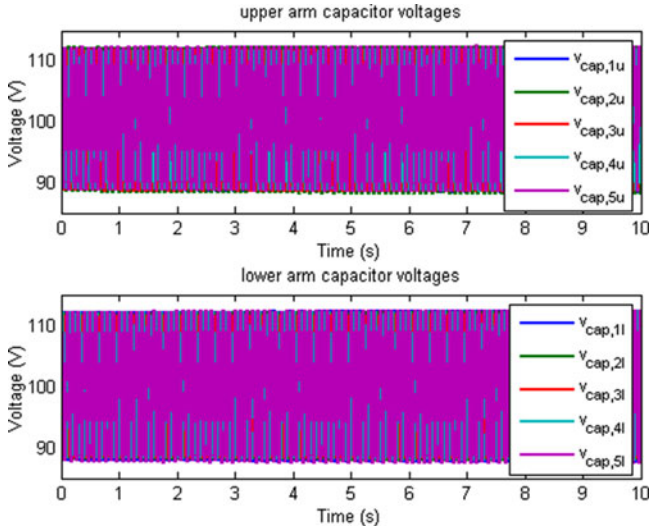

Fig. 18. Measured capacitor voltages in the upper (upper) and lower (lower) arms at $(N+1)$-level modulation.

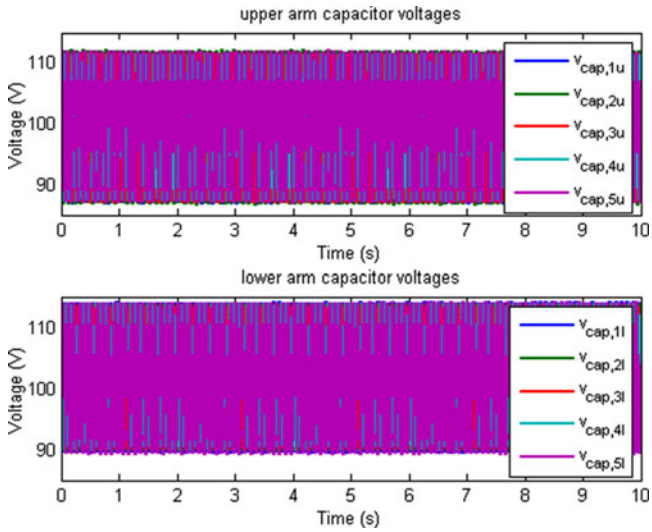

Fig. 19. Measured capacitor voltages in the upper (upper) and lower (lower) arms at $(2N+1)$-level modulation.

observed that for the 120-Hz switching frequency, there is a fundamental frequency component and odd-order harmonics in the ac-side voltage waveform. However, at the 130-Hz switching frequency, there are even-order harmonics, including a direct component, in the alternating voltage.

B. Experimental Results

The experimental results are carried out on the prototype shown in Fig. 12. The prototype has five submodules per arm and the switching frequency is 110 Hz. Accordingly, the product of the switching frequency and the number of submodules per arm is an odd multiple of the fundamental frequency. This means that balanced operating conditions are expected for $(N+1)$-level modulation, but not for $(2N+1)$-level modulation. This is validated by measuring the arm currents and capacitor voltages at both $(N+1)$-level and $(2N+1)$-level modulation. The measured arm-currents are shown in Fig. 13. As expected, the upper and lower arm current waveforms are similar but shifted in time when $(N+1)$-level modulation is used. However, when $(2N+1)$-level modulation is used, the current waveforms look different due to the odd-order harmonics in the circulating currents. The arm currents are also shown in Fig. 14 over a longer period of time. As expected, there are no signs of the currents changing over time as steady-state operation is considered.

The sum of the capacitor voltages in the upper and lower arms is shown in Fig. 15 for $(N+1)$-level modulation and Fig. 16 for $(2N+1)$-level modulation. The capacitor voltages appear to be stable in both cases. However, as expected, there is a difference between the upper and lower arm capacitor voltages when $(2N+1)$-level modulation is used. A more detailed view

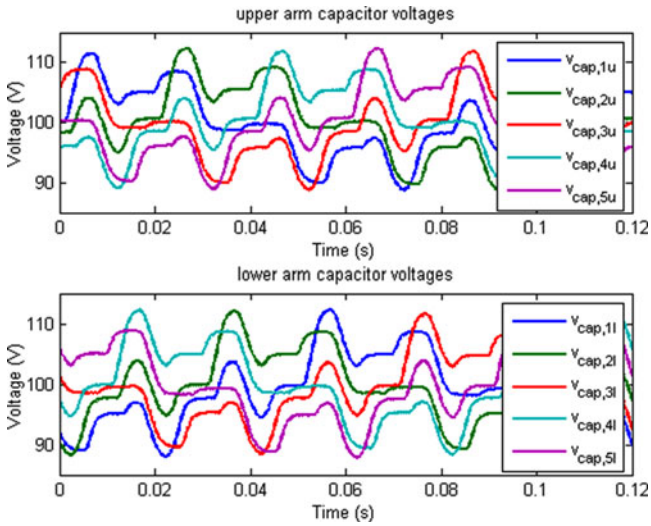

Fig. 20. Measured capacitor voltages in the upper arm (upper) and lower arm (lower) at $(N+1)$-level modulation.

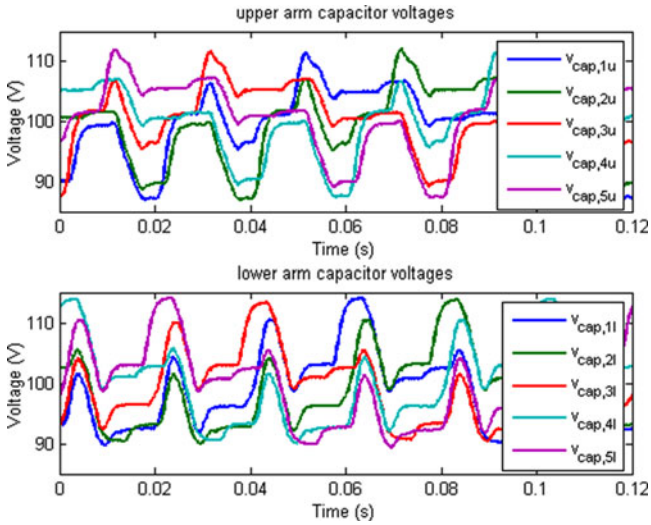

Fig. 21. Measured capacitor voltages in the upper arm (upper) and lower arm (lower) at $(2N+1)$-level modulation.

of v_{cu}^{Σ} and v_{cl}^{Σ} is given in Fig. 17. It is observed that it is not only the envelopes of v_{cu}^{Σ} and v_{cl}^{Σ} that are different at $(2N+1)$-level modulation, but also the shape of the waveforms.

The individual capacitor voltages are shown in Fig. 18 for $(N+1)$-level modulation and in Fig. 19 for $(2N+1)$-level modulation. As expected, no clear differences can be observed for $(N+1)$-level modulation. However, when $(2N+1)$-level modulation is used, the peak voltage in the lower arm capacitor voltages is slightly higher. A more detailed view of the capacitor voltages is shown in Fig. 20 for $(N+1)$-level modulation and Fig. 21 for $(2N+1)$-level modulation. As expected, for $(N+1)$-level modulation, the voltage waveforms are roughly the same in the upper and lower arms, but shifted in time. At $(2N+1)$-level modulation, the voltage waveforms are clearly different in the upper and lower arms. The capacitor voltages are, however, well balanced within each arm in both cases.

VI. Conclusion

This paper presents an analysis of the interaction between the switching harmonics, capacitor voltages, and arm and line quantities for the case when phase-shifted carrier modulation is used. The impact of the switching harmonics on the individual capacitor voltages is considered and it is found that in order to avoid diverging capacitor voltages, the switching frequency should not be an integer multiple of the fundamental frequency. The product of the number of submodules per arm and the switching frequency may, however, be an integer multiple of the fundamental frequency. In such a case, the arm and line quantities will be periodic with the fundamental frequency. This means that even if there are significant subharmonics in the capacitor voltages, no subharmonics will appear in the arm and line quantities for the given conditions. It is also found that odd- and even-order harmonics can be separated in such a way that the even-order harmonics appear on the dc side and the odd-order harmonics appear at the ac terminal. This is advantageous due to the fact that such a separation yields balanced operating conditions in the upper and lower arms. A more detailed description of how the switching frequency should be chosen in order to separate the odd- and even-order harmonics in the aforementioned fashion is presented in this paper. Thus, this study can be used to determine suitable switching frequencies for which capacitor voltages can be kept balanced, arm and line quantities will be periodic, and the operating conditions in the upper and lower arms will be symmetric. The theoretical results were validated by both simulations and experimental results.

References

[1] A. Lesnicar and R. Marquardt, "An innovative modular multilevel converter topology suitable for a wide power range," in *Proc. IEEE Bologna Power Tech*, Jun. 2003, vol. 3.

[2] S. Allebrod, R. Hamerski, and R. Marquardt, "New transformerless, scalable modular multilevel converters for HVDC-transmission," in *Proc. IEEE Power Electron. Spec. Conf.*, Jun. 2008.

[3] D. Peftitsis, G. Tolstoy, A. Antonopoulos, J. Rabkowski, J.-K. Lim, M. Bakowski, L. Ängquist, and H.-P. Nee, "High-power modular multilevel converters with SiC JFETs," in *Proc. IEEE Energy Convers. Congr. Expo.*, Sep. 2010.

[4] M. Hiller, D. Krug, R. Sommer, and S. Rohner, "A new highly modular medium voltage converter topology for industrial drive applications," in *Proc. Eur. Conf. Power Electron. Appl.*, Sep. 2009.

[5] A. Antonopoulos, K. Ilves, L. Ängquist, and H.-P. Nee, "On interaction between internal converter dynamics and current control of high-performance high-power ac motor drives with modular multilevel converters," in *Proc. IEEE Energy Convers. Congr. Expo.*, Sep. 2010.

[6] M. Hagiwara, K. Nishimura, and H. Akagi, "A medium-voltage motor drive with a modular multilevel PWM inverter," *IEEE Trans. Power Electron.*, vol. 25, no. 7, pp. 1786–1799, Jul. 2010.

[7] A. J. Korn, M. Winkelnkemper, and P. Steimer, "Low output frequency operation of the modular multi-level converter," in *Proc. IEEE Energy Convers. Congr. Expo.*, Sep. 2010.

[8] M. Winkelnkemper, A. Korn, and P. Steimer, "A modular direct converter for transformerless rail interties," in *Proc. IEEE Int. Ind. Electron. Symp.*, Jul. 2010.

[9] L. Ängquist, A. Haider, H.-P. Nee, and H. Jiang, "Open-loop approach to control a modular multilevel frequency converter," in *Proc. Eur. Conf. Power Electron. Appl.*, Aug./Sep. 2011.

[10] A. Antonopoulos, L. Ängquist, and H.-P. Nee, "On dynamics and voltage control of the modular multilevel converter," in *Proc. Eur. Conf. Power Electron. Appl.*, Sep. 2009.
[11] M. Perez and J. Rodriguez, "Generalized modeling and simulation of a modular multilevel converter," in *Proc. IEEE Int. Symp. Ind. Electron., Jun. 2011*, pp. 1863–1868.
[12] S. Rohner, J. Weber, and S. Bernet, "Continuous model of modular multilevel converter with experimental verification," in *Proc. IEEE Energy Convers. Congr. Expo.*, Sep. 2011.
[13] L. Harnefors, A. Antonopoulos, S. Norrga, L. Angquist, and H.-P. Nee, "Dynamic analysis of modular multilevel converters," *IEEE Trans. Ind. Electron.*,, vol. 60, no. 7, pp. 2526–2537, Jul. 2013.
[14] K. Ilves, A. Antonopoulos, S. Norrga, and H.-P. Nee, "Steady-state analysis of interaction between harmonic components of arm and line quantities of modular multilevel converters," *IEEE Trans. Power Electron.*, vol. 27, no. 1, pp. 57–68, Jan. 2012.
[15] K. Ilves, A. Antonopoulos, S. Norrga, and H.-P. Nee, "A new modulation method for the modular multilevel converter allowing fundamental switching frequency," *IEEE Trans. Power Electron.*, vol. 27, no. 8, pp. 3482–3494, Aug. 2012.
[16] A. Hassanpoor, S. Norrga, H.-P. Nee, and L. Ängquist, "Evaluation of different carrier-based PWM methods for modular multilevel converters for HVDC application," in *Proc. IEEE 38th Annu. Conf. Ind. Electron. Soc.*, 2012.
[17] Q. Tu and Z. Xu, "Impact of sampling frequency on harmonic distortion for modular multilevel converter," *IEEE Trans. Power Del.*, vol. 26, no. 1, pp. 298–306, Jan. 2011.
[18] P. Hu, D. Jiang, Y. Liang, Y. Zhou, Z. Lin, and J. Guo, "Zero tracking error nearest level modulation for modular multilevel converters," in *Proc. IEEE Annu. Conf. Ind. Electron. Soc.*, Nov. 2013.
[19] M. A. Perez, J. Rodriguez, E. J. Fuentes, and F. Kammerer, "Predictive control of ac–ac modular multilevel converters," *IEEE Trans. Ind. Electron.*, vol. 59, no. 7, pp. 2832–2839, Jul. 2012.
[20] A. Hassanpoor, K. Ilves, S. Norrga, L. Angquist, and H.-P. Nee, "Tolerance-band modulation methods for modular multilevel converters," in *Proc. Eur. Conf. Power Electron. Appl.*, 2013.
[21] M. Hagiwara, R. Maeda, and H. Akagi, "Control and analysis of the modular multilevel cascade converter based on double-star chopper-cells (MMCC–DSCC)," *IEEE Trans. Power Electron.*, vol. 26, no. 6, pp. 1649–1658, Jun. 2011.
[22] G. Konstantinou, M. Ciobotaru, and V. Agelidis, "Analysis of multi-carrier PWM methods for back-to-back HVDC systems based on modular multilevel converters," in *Proc. IEEE Annu. Conf. Ind. Electron. Soc.*, Nov. 2011.
[23] H. Peng, M. Hagiwara, and H. Akagi, "Modeling and analysis of switching-ripple voltage on the dc link between a diode rectifier and a modular multilevel cascade inverter (MMCI)," *IEEE Trans. Power Electron.*, vol. 28, no. 1, pp. 75–84, Jan. 2013.
[24] B. Jacobson, P. Karlsson, G. Asplund, L. Harnefors, and T. Jonsson, "VSC-HVDC transmission with cascaded two-level converters," in *CIGRE Session*, Aug. 2010.
[25] R. Marquardt, "Modular multilevel converter: An universal concept for HVDC-networks and extended dc-bus-applications," in *Proc. Int. Power Electron. Conf.*, Jun. 2010.
[26] M. Hagiwara and H. Akagi, "Control and experiment of pulsewidth-modulated modular multilevel converters," *IEEE Trans. Power Electron.*, vol. 24, no. 7, pp. 1737–1746, Jul. 2009.
[27] S. Bowes and B. Bird, "Novel approach to the analysis and synthesis of modulation processes in power convertors," *Proc. Inst. Electr. Eng.*,, vol. 122, no. 5, pp. 507–513, May1975.

Kalle Ilves (S'10) received the M.Sc. and Licentiate degrees in electrical engineering from the Royal Institute of Technology (KTH), Stockholm, Sweden, in 2009 and 2012, respectively, where he is currently working toward the Ph.D. degree in the Department of Electrical Machines and Power Electronics, since 2010.

His main research interests includes high-power converters for grid applications.

Lennart Harnefors (S'93–M'97–SM'07) was born in Eskilstuna, Sweden, in 1968. He received the M.Sc., Licentiate, and Ph.D. degrees in electrical engineering from the Royal Institute of Technology (KTH), Stockholm, Sweden, and the Docent degree in industrial automation from Lund University, Lund, Sweden, in 1993, 1995, 1997, and 2000, respectively.

Between 1994–2005, he was with Mälardalen University, Västerås, Sweden, where he held the positions of Research Assistant, Senior Lecturer, and, from 2001, Professor. He served as the Head of the Systems, Control, and Power Engineering Laboratory during 1998–2004. Between 2001 and 2005, he was, in addition, a Part-Time Visiting Professor of electrical drives with Chalmers University of Technology, Göteborg, Sweden. Since 2005, he has been with ABB, where he served in various capacities at the Grid Systems/HVDC business unit during 2005–2012. He is currently a Senior Principal Scientist at Corporate Research, Västerås, Sweden. He is with KTH as a Part-Time Adjunct Professor of power electronics. His research interests include analysis and control of power electronic systems, particularly grid-connected converters and ac drives. He is the author of more than 100 papers and holds five granted patents with several more pending.

Dr. Harnefors received the 2000 ABB Gunnar Engström Energy Award and the 2002 IEEE TRANSACTIONS ON INDUSTRIAL ELECTRONICS Best Paper Award. He is an Associate Editor of the IEEE TRANSACTIONS ON INDUSTRIAL ELECTRONICS, and a member of the Editorial Board of *IET Electric Power Applications* and the Executive Council and the International Scientific Committee of the European Power Electronics and Drives Association.

Staffan Norrga (M'00) was born in Lidingö, Sweden, in 1968. He received the M.Sc. degree in applied physics from the Linköping Institute of Technology, Linköping, Sweden, in 1993, and the Ph.D. degree in electrical engineering from the Royal Institute of Technology (KTH), Stockholm, Sweden, in 2005.

Between 1994 and 2011, he was a Development Engineer at ABB, Västerås, Sweden, in various power-electronics-related areas such as railway traction systems and converters for HVDC power transmission systems. In 2000, he returned to academia to engage in research on new power electronic converters employing soft switching and medium-frequency transformers at the Department of Electric Machines and Power Electronics, KTH, where he is currently an Associate Professor. His research interests include new converter topologies for power transmission applications and grid integration of renewable energy sources. He is the inventor or coinventor of 13 granted patents and 12 patents pending and has authored or coauthored more than 40 scientific papers published at international conferences or in journals with peer review.

Hans-Peter Nee (S'91–M'96–SM'04) was born in Västers, Sweden, in 1963. He received the M.Sc., Licentiate, and Ph.D. degrees in electrical engineering from the Royal Institute of Technology (KTH), Stockholm, Sweden, in 1987, 1992, and 1996, respectively.

In 1999, he was appointed as a Professor of power electronics at KTH, where he currently serves as the Head of the Electrical Energy Conversion Laboratory. His current research interests include power electronic converters, semiconductor components, and control aspects of utility applications, such as flexible ac transmission systems and high-voltage dc transmission, and variable-speed drives.

Dr. Nee received the Energy Prize by the Swedish State Power Board in 1991, the ICEM'94 (Paris) Verbal Prize in 1994, the Torsten Lindström Electric Power Scholarship in 1996, and the Elforsk Scholarship in 1997. He is a member of the European Power Electronics and Drives Association, involved with the Executive Council and the International Scientific Committee. He is also an Associate Editor of the IEEE TRANSACTIONS ON POWER ELECTRONICS and was on the board of the IEEE Sweden Section for several years, serving as its Chairman during 2002–2003.